MACF1 Facilitates SMAD7 Nuclear Translocation to Drive Bone Formation in Mice

Fan Zhao[1,a], Xiaoli Ma[1,a], Wuxia Qiu[1], Pai Wang[1], Ru Zhang[1], Zhihao Chen[1], Peihong Su[1], Yan Zhang[1], Dijie Li[1], Jianhua Ma[1], Chaofei Yang[1], Lei Chen[1], Chong Yin[1], Ye Tian[1], Lifang Hu[1], Yu Li[1], Ge Zhang[2], Xiaoyang Wu[3], Airong Qian[1, b, #]

[1] Lab for Bone Metabolism, Key Lab for Space Biosciences and Biotechnology, School of Life Sciences; Research Center for Special Medicine and Health Systems Engineering; NPU-UAB Joint Laboratory for Bone Metabolism, Northwestern Polytechnical University, Xi'an, Shaanxi 710072, China.

[2] Law Sau Fai Institute for Advancing Translational Medicine in Bone and Joint Diseases, School of Chinese Medicine, Hong Kong Baptist University, 999077, Hong Kong, SAR, China.

[3] The University of Chicago, Ben May Department for Cancer Research, Chicago, Illinois 60637, USA.

[a] These authors contributed equally to this work.

[b] Lead Contact

[#] Correspondence: qianair@nwpu.edu.cn

KEYWORDS

MACF1, bone development, bone formation, mesenchymal stem cells, osteogenic differentiation, cytoskeleton, SMAD7

ABSTRACT

MACF1 is a large crosslinker that contributes to cytoskeleton integrity and cell differentiation. Loss of MACF1 impairs multiple cellular functions in neuron development and epidermal migration, and is the molecular basis for many diseases such as heart failure and Parkinson's disease. MACF1 is highly abundant in bones, however, its involvements in osteogenic differentiation and bone formation are still unknown. In this study, by conditional gene targeting to delete the *Macf1* gene specifically in MSCs, we observed ossification retardation and bone loss in MACF1 deficient mice in different developmental stages, which we traced to disorganized cytoskeleton and decreased osteogenic differentiation capability in MSCs. Further, we show that MACF1 interacts and facilitates SMAD7 nuclear translocation to initiate downstream transcription. These findings are hopefully to expand the biological scope of MACF1 in bones, and provide experimental basis for targeting MACF1 in degenerative bone diseases such as osteoporosis.

INTRODUCTION

The microtubule-actin cross-linking factor 1 (MACF1) is an important mammalian spectraplakin protein that interacts with the cytoskeleton (Ka et al., 2014; Leung et al., 1999; Suozzi et al., 2012). As one of the largest mammalian protein (~ 620 KD) that coordinates the cytoskeleton, MACF1 has the ability to bind to actin filaments with its N-terminal calponin homology domain, and interact with microtubules with the C-terminal GAR/GSRA domain (Lane et al., 2017; Leung et al., 1999) (Figure EV1A). MACF1 also has cation binding sites in the C-terminus (Figure EV1A), and homologous sequence similar to the Smc family of ATPases (Lane et al., 2017; Wu et al., 2008), suggesting considerable potential kinase activity. In addition, MACF1's cytoskeletal crosslinking capability together with its ATPase activity enable growth of the MTs toward focal adhesions (FAs), which facilitates cell migration and polarization (Wu et al., 2008). MACF1 mainly localizes in the cytoplasm, and is reported to participates in MT-mediated cargo transport (Chen et al., 2006; Kakinuma et al., 2004; Wu et al., 2008). MACF1 is also found in the nucleus, a few MACF1 goes to the nucleus from the cytoplasm.

MACF1 is expressed ubiquitously as early as at E7.5 during embryonic period (Chen et al., 2006), and plays essential roles in regulating various development processes in

2

mammals (Antonellis et al., 2014; Ka and Kim, 2016; May-Simera et al., 2016). With especially high abundance in the heart, lung, brain and bones, its unique structure enables MACF1 a variety of functions in neuron development, epidermal migration and more (Duhamel et al., 2018; Escobar-Aguirre et al., 2017; Yue et al., 2016), analysis of these evidences show that MACF1 is crucial for normal cells to proliferate, polarize and differentiate. Reduction or depletion of MACF1 disorganizes the cytoskeleton and impairs cellular functions (Escobar-Aguirre et al., 2017; Ka et al., 2016; Ma et al., 2017; Wang et al., 2017), and further confers risk for degenerative diseases such as inflammatory colitis and Parkinson's disease (Ka and Kim, 2016; Kodama et al., 2003; Ma et al., 2017; Wang et al., 2017).

However, the function of MACF1 is less understood in bones. The bones are rigid structural support and endocrine organ in mammals. During early embryonic development, osteoprogenitors aggregate and differentiate into osteoblasts to synthesize new bone matrix and form flat bones such as the skull, while replacement of the cartilage tissue by ossified bone forms long bones such as the femur. In adults, bone metabolism is dynamicly regulated by osteoblasts-mediated bone formation and osteoclasts-mediated bone resorption (Khurana, 2009). MACF1 is also highly abundant in the bone tissue, but its functions in the regulation of bone development and formation remains unknown. Considering the vital roles MACF1 play in other tissues, the lack of information on MACF1's function in bone tissue needs to be addressed, we wonder how MACF1 regulates bone development and formation. In addition, as a key cytoskeletal regulator, we wonder in particular how MACF1 affects the cytoskeleton in bone-forming cells and controls osteogenic differentiation. Our earlier studies show that knockdown of MACF1 in preosteoblasts inhibited osteoblast differentiation (Hu et al., 2017, 2015), and femoral *Macf1* level is significantly lower in osteoporotic mice (Yin et al., 2018) and is also negatively correlated to the age of mice (Hu et al., 2017), suggesting a close relationship between MACF1 and osteoporosis. Therefore, we hypothesize that MACF1 is essential for maintaining the cytoskeleton in mesenchymal stem cells (MSCs), and positively regulates osteogenic differentiation and bone formation.

In this study, we unveiled essential roles of MACF1 in osteogenic differentiation and bone formation *in vivo*. By genetical manipulation to delete MACF1 in the

3

79   mesenchyme, we identified essential roles of MACF1 in regulating osteogenic differentiation

80   and bone formation in mice. We show that MACF1 is essential for early stage bone

81   development, loss of MACF1 in MSCs retards bone development and further impairs bone

82   properties and bone strength. *In vitro* experiments demostrate that MACF1 is essential for

83   maintaining the cytoskeleton in differentiating MSCs, loss of MACF1 disorganizes the

84   cytoskeleton and inhibit osteogenic differentiation. In addition, we show that MACF1 directly

85   interacts with SMAD7 and facilitates SMAD7 nuclear translocation to initiate downstream

86   osteogenic pathways. By coupling the results obtained, we have identified key roles of

87   MACF1 in maintaining osteogenic differentiation and bone formation, and advanced the

88   potential for exploiting MACF1 as a new therapeutic target for degenerative bone diseases

89   such as osteoporosis.

Results

Mesenchymal deletion of MACF1

92   MACF1 is a large structural protein (Bernier et al., 1996; Leung et al., 1999). Previous

93   studies show that conventional inactivation of the *Macf1* gene leads to teratogenicity and

94   lethality during development (Chen et al., 2006), suggesting MACF1 is crucial for embryo

95   development in mice. In order to study the *in vivo* involvement of MACF1 in bone

96   development and formation, we utilized the Cre/Loxp technology and generated a

97   genetically modified mouse model in which the *Macf1* gene was specifically deleted in

98   mesenchymal stem cells (Flox, Macf1$^{f/f}$; cKO, Macf1$^{f/f}$;Prx1$^{Cre/+}$) (Figure EV1A and S1B).

99   Similar to those conditional MACF1 deficient mice generated using other Cre lines,

100 mesenchymal deletion of MACF1 did not significantly affect body length or body weight in

101 neonates (Figure 1A, Figure EV1C) (Goryunov et al., 2010), and offsprings were obtained

102 in an expected sex ratio and Mendelian frequency (Figure EV1D), By adulthood, body size

103 and organ coefficient remained unchanged as well (Figure 1B, S1E and S1F), suggesting

104 that mesenchymal deletion of MACF1 did not apparently change fundamental physiological

105 indications in mice.

106 We then detected MACF1 expression levels to confirm successful deletion of MACF1.

107 Real-time quantitative PCR (qPCR) assays for detection of tissue *Macf1* levels showed that

108 in the conditional knockout (cKO) group, the *Macf1* gene level was significantly lower in bone

4

109 tissue, while in other tissues like muscle, cerebrum and liver, *Macf1* mRNA levels remained
110 unchanged compared with control mice (Figure 1D). It may be worth noting that mRNA level
111 of the *Macf1* gene was also lower in the brown adipose tissue (Figure 1D). Then
112 immunoblotting and immunofluorescence experiments further demonstrated that MACF1
113 protein was barely detectable in MACF1 cKO MSCs (Figure 1E). The results indicate that
114 conditional targeting of MACF1 was successful, and that mesenchymal deletion of MACF1
115 does not change fundamental physiological indications in mice.

116 Mesenchymal deletion of MACF1 impairs early-stage bone development in mice

117 Previous studies report that Prx1-driven (paired related homeobox 1) Cre recombinase
118 is expressed in a subset of craniofacial mesenchyme and in early limb bud mesenchyme
119 (Elefteriou and Yang, 2011; Logan et al., 2002). To study the impact of MACF1 on bone
120 development in mice, we first examined skull development and morphology at late
121 embryonic stage as well as in neonatal mice. Cleared skeletal preparation of the skull
122 showed that the cKO neonates displayed obvious retardation in cranial bone development
123 at E19.5 and P1, manifested as delays in suture fusion and calvarial ossification (Figure 1E,
124 1F and S2A). MicroCT experiment again substantiated the retardation in suture closure, and
125 found that parietal bone was thinner in cKO mice at P1 (Figure 2C and 2D). In addition,
126 formalin-fixed paraffin embedded (FFPE) skull sections were also prepared. HE staining
127 confirmed attenuation in calvaria thickness, while alkaline phosphatase (ALP) staining
128 showed that cKO mice had less ALP expression in parietal bone (Figure 2E), but Alcian blue
129 staining didn't show significant difference between Flox and cKO mice (Figure EV2E),
130 suggesting decreased osteoblastic activity in MACF1 deficient mice during cranial bone
131 development.

132 Unlike flat bones, bones of the trunk and extremities are formed with an initial hyaline
133 cartilage. To further investigate the effect of MACF1, long bones were also scrutinized.
134 Cleared bone preparation for long bones revealed that mineralized bone formation in tibia
135 was also slower due to MACF1 deletion (Figure EV2C and S2D), while other long bones
136 such as ribs and forelimbs were less affected (Figure EV2C and S2D), indicating that, to
137 some extent, development and formation of the lone bones in neonatal mice were also
138 affected due to MACF1 deletion. The results suggest that MACF1 is crucial for early-stage
139 development and formation of the skeleton in mice.

5

Loss of MACF1 weakens bone properties in adult mice

Bone forming cells derived from mesenchymal stem cells are responsible for bone matrix synthesis and mineralization (Hilton, 2014), and finally form the mineral structure that supports bone functions. To investigate the involvement of MACF1 on bone phenotype during adulthood, bone properties in MACF1 deficient mice were tested. Firstly, 3-month old mice were subjected to dual energy X-ray absorptiometry (DEXA) scanning, the results showed that mineral density was lower in both femur and third lumbar vertebra (Figure 2A), bone mineral content and bone volume were also lower (Figure EV3A).

Next, distal femur from 6-week old male mice were scanned and reconstructed by microCT. The results showed that in cKO mice, bone mineral content and mineral density were lower (Figure 2B and 2C), manifest as decreased trabecular number, thickness and increased trabecular spacing (Figure 3D), indicating that MACF1 deletion decreased bone mass, and degenerated bone microarchitecture. In addition, to known mechanical properties of the bone, freshly-isolated femora were subjected to 3-point bending test. We found in cKO group not only reduced maximum compression stress and compression strain, but also reduced Young's elastic modulus (Figure 3E), suggesting that toughness and strength of the bone were weakened in cKO mice.

Bone microenvironment changes with age, and accordingly, the regulation of MSCs osteogenic differentiation varies as well. To confirm age-related phenotypes of the MACF1 deficient mice, mice older than peak bone mass age (around 6 month) were examined. MicroCT analysis of 7-month old distal femur showed that in cKO mice, bone mass and bone volume were significantly lower than those in Flox mice (Figure 2F), together with deteriorated trabecular microarchitecture (Figure EV3B). Further, H&E staining of FFPE femur sections showed that in 12-month mice, trabecular bone volume of cKO mice was still lower (Figure 2G), and marrow adipocyte number increased in MACF1 deficient mice (Figure EV3C). It is worth noting that, with increased age, BV/TV disparity between Flox and cKO mice increased from 23.9% at 6w to 35.7% at 12m (Figure 2C, 2F and 2G), suggesting that loss of MACF1 impairs bone properties more seriously in aged mice. Together, these results suggest that MACF1 positively regulates bone mass and bone quality in mice, and that loss of MACF1 confers risk for osteoporosis and fracture.

MACF1 is required for bone formation

6

Osteoblasts and osteoclasts are two main cell types in mature bone tissue that synthesize or decompose bone matrix to coordinate bone remodeling. To further understand the behavior of MACF1 in bone development, histochemistry approaches were utilized. Firstly, to differentiate mineralized bone from osteoid that undergoing rapid bone growth, undecalcified femur sections (plastic sections) from 6-week old male mice were prepared. The Goldner's trichrome staining results showed that in addition to porotic and lesser trabeculae, the cKO mice also showed atypical accumulated osteoid on surfaces of both the trabecular and cortical bone (Figure 3A and 3B).

Certain substances produced during bone remodeling are secreted into peripheral blood, and could be used as biomarkers to reflect osteoblast function, osteoclast function and metabolic rate of the bone. We next quantified bone metabolism-related serological factors in same old male mice, and found that bone formation-related factors such as osteocalcin (OCN) were decreased in cKO mice, while bone resorption-related factors like carboxy-terminal collagen crosslinks (CTX) level were elevated (Figure 3C), suggesting reduced bone matrix mineralization and increased type I collagen decomposition due to MACF1 deletion. Furthermore, FFPE sections were also prepared and stained for tartrate-resistant acid phosphatase (TRAP). Consistent with earlier results, the cKO mice showed accumulated TRAP expression on bone surfaces (Figure 3D and S4A).

Lastly, to see the dynamic action of MACF1 on bone formation, mice at 6-week old and 3-month old were double-labeled with calcein, respectively. Fluorescence imaging of plastic sections showed that, regardless of mice age, femoral mineral apposition was slower in cKO mice (Figure 3E and S4B). Bone histomorphometric analysis further revealed that matrix mineralization and bone formation on bone surfaces were also slower (Figure 3F and S4B). These data suggest that MACF1 is required for bone formation in mice; insufficient MACF1 shifts the balance of bone remodeling and finally impairs bone formation.

Loss of MACF1 disorganizes the cytoskeleton in MSCs

As a large structure protein, MACF1 interacts with microtubule and microfilaments simultaneously to coordinates cytoskeleton during cell proliferation and differentiation, and is reported to stabilize the cytoskeleton in different cell types (Fassett et al., 2013; Wang et al., 2017; Wu et al., 2008; Yue et al., 2016). To investigate the cytoskeletal role of MACF1 during osteogenic differentiation, MSCs from MACF1 deficient mice were isolated and

analyzed. Immunofluorescence staining using antibody recognizing the alpha-tubulin showed in Flox cells distinct microtubule organizing center (MTOC), and ordered and well-organized microtubule filaments (Figure 4A), whereas in cKO cells, the MTs appeared to be acentric, MTOC disappeared, and the morphology of non-centrosomal microtubules became disorganized and cluttered (Figure 4A). Morphometric analysis of the microtubule demonstrated that mesenchymal deletion of MACF1 decreased anisotropy of MT filaments, and more importantly, depolarized orientation of the microtubule (Figure 5B), suggesting loss of MACF1 in MSCs impairs organization and structural regularity of the microtubule cytoskeleton. Next, we analyzed the actin cytoskeleton. Unlike the action of MACF1 to microtubule, loss of MACF1 did not seem to significantly affect the actin filaments (Figure 4C), similar anisotropy and orientation of the actin filament were found between cKO cells and Flox cells (Figure 4D).

Focal adhesions (FAs) are end parts of the F-actin that extend into the extracellular matrix. It is reported that MACF1 specifically promotes the crosslinking of microtubule and microfilament, and guide growth of the microtubule plus-ends towards FAs (Stehbens and Wittmann, 2012; Wu et al., 2008). To further understand the action of MACF1 on the cytoskeleton, FAs in MACF1 deficient MSCs were stained and analyzed. Immunofluorescence staining using antibodies recognizing vinculin or paxillin showed that, upon MACF1 deletion, the size of FAs increased significantly, and morphology of FAs changed from spindle-shaped in Flox cells to filament-like in cKO cells (Figure 4E and 4F), and the number of focal adhesions also increased in cKO cells (Figure 5F), indicating increased spread area of focal adhesions in cKO MSCs. These results suggest that MACF1 is necessary for maintaining microtubule integrity and focal adhesion morphology to coordinate cytoskeleton in MSCs.

Loss of MACF1 inhibits osteogenic differentiation in MSCs

Although the *in vitro* roles of MACF1 have been studied in cells such as neuron and epidermis cell, much is still unknown about its *in vivo* functions in bone forming cells. To study the involvement of MACF1 in MSCs during osteogenic differentiation, we isolated and cultured bone-derived MSCs from the MACF1 cKO mice. Firstly, differentiation capability of MSCs during osteogenic induction was assayed. Von Kossa staining showed that at 21st day of osteo-induced culture, loss of MACF1 greatly inhibited mineralization capability in

MSCs (Figure 5A). In addition, alkaline phosphatase (ALP) and Alizarin Red S (ARS) staining further verified that during osteo-induction, MSCs lack of MACF1 had less ALP activity and less mineralized nodule formation (Figure 5B, C and S6A), indicating inhibited osteogenic differentiation capability.

Next, proliferation and differentiation capability of differentiating MSCs were detected non-invasively by electric cell-substrate impedance sensing (ECIS) assay. By monitoring real-time impedance values during osteo-induced culture, the ECIS curve showed that during exponential growth, proliferation capability decreased significantly in MACF1 deficient MSCs (Figure 5D, left), population doubling time increased from 39.8 h in Flox cells to 50.5 h in cKO cells. In addition, the ECIS curve reveled that loss of MACF1 significantly suppressed differentiation capability of MSCs, especially in early phase of osteogenic differentiation (Figure 5D, right).

Lastly, qPCR analysis revealed that, during osteogenic differentiation, levels of either *Macf1* or osteogenic genes decreased with induction time (Figure 5E), and more importantly, levels of both *Macf1* and osteogenic genes such as alkaline phosphatase (*Alpl*), collagenase 1 alpha 1 (*Col1a1*), osteocalcin (*Ocn*) and *Runx2* decreased significantly in MACF1 deficient cells (Figure 5E), suggesting impaired osteogenic differentiation capability upon MACF1 deletion. These data indicate that MACF1 is necessary for maintaining osteogenic differentiation, and lack of MACF1 would impairs osteogenic functions in MSCs.

MACF1 interacts with SMAD7 in MSCs

To explore novel downstream molecules that interact with MACF1 to regulate osteogenic differentiation, we performed iTRAQ-labeled proteomics experiment using MC3T3-E1 preosteoblasts. First we co-immunoprepacited cell lysate using anti-MACF1 antibody, and confirmed immunoprecipitation capability of the anti-MACF1 antibody (Figure 6A, S7A and S7B). Next, the IP products were labeled with iTRAQ reagent and subjected to liquid chromatography followed by tandem mass spectrometry (LC-MS/MS) analysis. Unique peptide analysis showed that there were more than 60 proteins interacting with MACF1 in MC3T3-E1 cells, among which 5 were transcription factors (TFs), i.e., BHLHE40, HES1, REL, SMAD7, ZFP748 (Figure 6B). To further verify the involvement of these TFs in osteogenic differentiation, the ToppGene database was used to predict their potentials in osteogenic regulation, and highlighted SMAD7 as a most likely transcription factor in

9

264   osteogenic regulation (data for ZFP748 not found) (Figure 6C, S7C and S7D). In addition,

265   qPCR analysis revealed that in MC3T3-E1 cells, *Smad7* still had relatively high abundance,

266   and in *Macf1* knockdown cells, *Smad7* levels was also lower (Figure 6D). Lastly, we isolated

267   MSCs from wild type mice and performed co-IP to test SMAD7-MACF1 interaction in MSCs.

268   The results showed that SMAD7 was detectable in the immunoprecipitated product,

269   indicating interaction of MACF1 and SMAD7 in MSCs (Figure 6E). Besides,

270   immunofluorescence showed from the perspective of intracellular distribution co-localization

271   of MACF1 and SMAD7, which in turn confirmed the Co-IP result (Figure 6F).

272   On the basis of MACF1-SMAD7 interaction, to further clarify their regulatory pattern in

273   osteogenic differentiation, we manipulated MACF1 expression in a variety of cell lines and

274   tested SMAD7 expressions in both the cytoplasm and nucleus. Firstly, in Floxed MSCs, we

275   found that MACF1 was mostly expressed in the cytoplasm, and upon MACF1 deletion,

276   expression of MACF1 decreased significantly in both the cytoplasm and nucleus. Similar to

277   the MACF1 expression pattern, SMAD7 also expressed mostly in cytoplasm, and deletion

278   of MACF1 significantly decreased expression of SMAD7, especially in the nucleus (Figure

279   6G, left). Next, we constructed a *Macf1* knockdown (MACF1-shRNA) MC3T3-E1 cell line,

280   and found in KD cells reduced expression of SMAD7 (Figure 6G, middle). Lastly, we

281   constructed a cell line to restore MACF1 expression by transfection of pKH3S-ACF7 plasmid

282   into the *Macf1* knockdown cells, and found that, as compared with empty plasmid control

283   group, restoration of MACF1 significantly elevated SMAD7 levels, especially in the nucleus

284   (Figure 6G, right). These data suggest that, in bone forming cells, SMAD7 interacts with

285   MACF1 and shares a similar expression trend.

286   MACF1 facilitates nucleus translocation of SMAD7 to drive osteogenic differentiation

287   SMAD7 is a key member of the TGFβ superfamily SMAD family that regulates cell

288   metabolism. Studies show that, SMAD7 may play versatile roles in cell signaling.

289   Cytoplasmic SMAD7 was found to inhibit cellular functions (e.g. in bone forming cells) (Wu

290   et al., 2016), while nuclear SMAD7 was reported to promote cellular functions (e.g. in

291   myoblasts) (Miyake et al., 2010). Still, there's no data to clarify the nuclear roles of SMAD7

292   in bone forming cells. To further clarify how SMAD7 participates in osteogenic regulation

293   through interacting with MACF1, we constructed a conventional SMAD7 overexpression

294   plasmid (pcDNA_SMAD7) and a nuclear localization signal-carrying SMAD7 overexpression

plasmid (pcDNA_SMAD7-NLS), respectively, to studied the subcellular functions of SMAD7 in MC3T3-E1 osteoblasts (Figure 7A).

Next, the transfection efficiency was examined. Immunofluorescence images showed that, 12 h after transfection, level of cellular SMAD7 increased, in cells transfected with conventional plasmid, SMAD7 distributed mostly within the cytoplasm, while in cells transfected with NLS-carrying plasmid, SMAD7 concentrated mostly within the nucleus (Figure 7B). Then, we explored the effects of SMAD7 overexpression on osteogenic differentiation. qPCR analysis revealed that, as compared with empty plasmid transfected group (Vec0), *Smad7* expression increased dramatically after transfected with two kinds of plasmids. In cells transfected with conventional SMAD7 plasmid, expressions of osteogenic genes such as *Col1a1* and *Alpl* decreased simultaneously, levels of osteogenic-related transcription factors reduced as well (Figure 7C). However, in cells transfected with NLS-carrying SMAD7 plasmid, levels of both osteogenic genes and transcription factors increased significantly (Figure 7C and S8A).

Lastly, cells transfected with plasmids were osteo-induced and stained for ALP. The results showed that, as compared with the empty plasmid transfected group, ALP activity decreased in conventional SMAD7 plasmid transfected cells, and increased in NLS-carrying plasmid transfected cells (Figure 7D). These results suggest that, during the process of osteogenic differentiation, cytoplasmic SMAD7 plays an inhibitory role, while nuclear SMAD7 positively regulates osteogenic functions. Concerning the evidence that SMAD7 interacts with MACF1, these data indicate that during osteogenic differentiation, MACF1 facilitates nuclear translocation of SMAD7 to drive downstream osteo-related signaling and to positively regulate bone formation.

DISCUSSION

In this study, we identified MACF1 as a key regulator that controls osteogenic functions in mice. We show that MACF1 is necessary for bone development and formation. Loss of MACF1 decreases bone mass and quality in adult mice, which confers risk for degenerative bone diseases such as fracture. In addition, MACF1 stabilizes the microtubule cytoskeleton and controls focal adhesion morphology and regulates osteogenic differentiation in MSCs. Although the role of MACF1 in material transportation has been reported, a novel

11

transcriptional factor SMAD7 that interacts directly with MACF1 is identified until this study, which initiates and promotes downstream osteogenic pathways. Our findings provide a new mechanism for understanding osteogenic differentiation and bone formation regulation, and identified MACF1 as a potential therapeutic target for degenarative bone diseases such as osteoporosis.

Essential roles of MACF1 in regulating bone development and formation

Conventional or nervous-tissue-specific knockout of MACF1 was reported to be embryonic lethal (Chen et al., 2006; Goryunov et al., 2010), but mesenchymal-specific MACF1 KO mice survived and are physically normal, suggesting a relatively independent role of MACF1 in bones. However, mice lacking MACF1 show different degrees of retardation in skull and long bone development. Considering the MACF1 deficiency phenotypes found in other tissues (Fassett et al., 2013; Goryunov et al., 2010; Ka et al., 2014; Ka and Kim, 2016; Liang et al., 2013; May-Simera et al., 2016), we believe that MACF1 is also responsible for positive regulation of bone growth and development. Loss of MACF1 would likely cause abnormalities during early stages of bone development.

In adult mice, especially with increased age, loss of MACF1 impairs bone mass, mineral density and bone properties tremendously, which experimentally confirmed MACF1 as a potential key regulator for degenerative bone disorders such as osteoporosis. Further investigations show that, loss of MACF1 inhibits bone surface mineralization capability, promotes osteoclasts functions and subsequently inhibits bone formation. Therefore, we propose that loss of MACF1 disrupts the balance of bone remodeling, and confers risk for degenerative bone diseases. Interestingly, MACF1 deficient mice have more osteoid deposited on bone surfaces, which is inconsistent with what we have hypothesized. Further serological analysis shows that MACF1 deficient mice have less ability to mineralize osteoid, elevated osteoid is likely to be produced in a compensatory manner, but insufficient MACF1 leads to insufficient mineralization capability, and finally leads to reduced bone mass.

Loss of MACF1 impairs cytoskeleton dynamics and osteogenic functions

As an important cytoskeleton regulator (Suozzi et al., 2012), we hypothesized that MACF1 also regulates the cytoskeleton in MSCs. Our results show that, loss of MACF1 disorganized the microtubule cytoskeleton and depolarized the cell. Previously, it is reported that loss of MACF1 disturbs the microtubule cytoskeleton in epidermis, neuron and

12

myoblasts, therefore we believe MACF1 is also important for maintaining the microtubule cytoskeleton in MSCs. The actin cytoskeleton is not the same, however, loss of MACF1 doesn't seem to affect the morphology or polarity of the actin filaments. Similar phenomenon was found in epithelial cells, in which MACF1 deletion affected the microtubule cytoskeleton, rather than the microfilaments, and it is the microfimants, rather than the MTs, that could reorganize themselves in the absence of MACF1 (Kodama et al., 2003). Considering the molecular structure of MACF1, a tentative inference on this difference is that MACF1 crosslinks differently with microtubules and microfilaments, respectively. Focal adhesions are essential parts of the cytoskeleton, we find that MACF1 deficient MSCs have larger and more focal adhesions. Earlier studies also show that loss of MACF1 stabilizes focal adhesions, impairs its dynamic characteristics and then affects cell motility (Ning et al., 2016; Wu et al., 2008; Yue et al., 2016). Taking together these results, we propose that MACF1 regulates focal adhesion morphology to control MSCs adhesion and motility.

Interaction of MACF1 and SMAD7 during osteogenic differentiation

MSCs differentiate into bone forming cells to support osteogenic functions. Based on the *in vivo* results, we hypothesized that loss of MACF1 impairs osteogenic functions in MSCs. The *in vitro* experiments validate that osteogenic differentiation capability in MSCs rely heavily on sufficient expression of the *Macf1* gene. There are also more studies to show that loss of MACF1 inhibits cell differentiation (Ka and Kim, 2016), which are attributed to disorganized cytoskeleton (Ka et al., 2014). Next, we identified SMAD7 as a downstream transcriptional factor that interacts with MACF1 to be translocated into the nucleus to initiate downstream osteogenic pathways. SMAD7 has been shown to regulate osteogenic functions. A prevailing view is that SMAD7 act as a repressor in the TGF-β/BMP signaling pathway (Miyazawa and Miyazono, 2017; Wu et al., 2016), but emerging evidences are presenting its positive roles in osteogenic regulation (Li et al., 2014). We noticed that this may be due to its subcellular localization, but the nuclear roles of SMAD7 are still unknown. On the one hand, SMAD7 exists simultaneously in the cytoplasm and nucleus in different types of cells. For instance, nuclear SMAD7 in myoblasts promotes myogenesis (Miyake et al., 2010), similar results are also found in fibroblasts and other cells (Emori et al., 2012). On the other hand, MACF1 is reported to have ATPase activity (Wu et al., 2008), and mediate intracellular material trafficking (Chen et al., 2006; Slep et al., 2005), our data show

13

387 that SMAD7 has multiple phosphorylation sites (Hornbeck et al., 2015), and MACF1 shuttles

388 between the cytoplasm and nucleus. For this reason, we overexpressed SMAD7 in MSCs,

389 and found nuclear-specific overexpression of SMAD7 promotes osteogenic differentiation,

390 while whole cell overexpression (in fact mostly accumulated in the cytoplasm) shows

391 inhibitory effects. By differentiate its subcellular roles, we uncover new function of SMAD7

392 in osteogenic differentiation regulation.

393   In summary, we discovered new roles of MACF1 in regulating osteogenic differentiation

394 and bone formation, loss of MACF1 in bone forming cells impairs osteogenic functions and

395 then leads to degenerative bone disorders such as osteoporosis. Further, we identified

396 SMAD7 as a key transcriptional factor that interact with MACF1 to be translocated into the

397 nucleus to initiate downstream osteogenic pathways.

MATERIALS AND METHODS

Generation of the MACF1 cKO mouse

400 Mice carrying the floxed MACF1 alleles (in B6 background) were acquired through a material

401 transfer agreement between the University of Chicago (USA) and the Northwestern

402 Polytechnical University (China). Construction of the targeting vector was reported

403 previously (Wu et al., 2008), in which the loxP sites were integrated to excise exon 11, 12

404 and 13 of the *Macf1* gene (while in the original literature, the flanked exons were reported

405 as E6 and E7) (Figure EV1A). Mice expressing Cre recombinase under the control of Prx1

406 promoter (in B6 background) were acquired from Biocytogen Co., Ltd. (Beijing, China). The

407 MACF1 conditional knockout mice were generated by breeding the MACF1 Flox mice to the

408 Prx1-Cre mice. Offspring genotype was determined by PCR analysis of genomic DNA from

409 the toe tissue (or for embryos, from liver tissue).

410 Feed and water used for mice husbandry were pre-processed properly (^{60}Co irradiated feed;

411 boiled water), and were all available *ad libitum* to mice. Breeding and number of mice were

412 controlled according to the 3Rs principle. Mice used for planned experiments were

413 euthanized after overdose injection of pentobarbital sodium (i.p., 1 g/Kg), while others

414 were euthanized by CO_2 inhalation. All mice experiments were performed according to the

415 *Guide for the Care and Use of Laboratory Animals* and under the permission of Laboratory

416 Animal Ethics & Welfare Committee of the Northwestern Polytechnical University.

Study design & animal grouping

To study the *in vivo* functions of MACF1, age-matched same-sex controls were set up (mice numbers are indicated in each figure). Unless otherwise stated, the MACF1[f/f];Prx1[Cre/+] mice (cKO) were considered to have the *Macf1* gene deleted specifically in MSCs, while the MACF1[f/f] mice (Flox) were used as controls. All mice were maintained in barrier condition (SPF lab, 12/12 h light cycle, 24 ± 1 °C, 30-70% RH) with no more than 4 in each cage.

Cell preparation

Mouse mesenchymal stem cells were isolated from compact bone of 6-week old male mice (Zhu et al., 2010). Briefly, mice femora were isolated, cleaned and transferred to a 60-mm culture dish containing 5 mL α-MEM (supplemented with 0.1% penicillin/streptomycin and 2% FBS). Epiphyses in both ends were cut open for complete removal of bone marrow. Bone shafts were then excised into chippings and digested (α-MEM + 10% FBS + 1 mg/mL Type II collagen, 37 °C, 200 rpm, 1h), bone chips were then collected and seeded in a 60-mm dish for culture (37 °C, 5% CO_2). Culture medium was changed on the third day to remove loosely attached cells and tissue debris. Cells at passage 2 to 5 were used for experiments.

Construction of the MACF1 knockdown MC3T3-E1 cell line (KD), and transfection of pKH3S-ACF plasmid into MACF1 KD cells were reported previously (Hu et al., 2015; Zhang et al., 2018).

Growth medium (10% FBS + 1% pen-strep + 1% L-glutamine in α-MEM) were used for subculture, and osteo-induction medium (10% FBS + 1% pen-strep + 1% L-glutamine + 0.1 μM dexamethasone + 50 μg/mL ascorbic acid + 10mM glycerol in α-MEM) were used for osteo-induction.

RNA and qPCR

High quality total RNA from cell and tissue samples were isolated using TRIzol™ reagent according to the manufacturer's instructions. RNA quality was determined by ultraviolet spectrophotometry. cDNA was synthesized on 1 μg total RNA using the cDNA synthesis kit (TaKaRa, Japan) following the manufacturer's instructions. Real-time quantitative PCR was performed using the SYBR® Green method on 2 μL cDNA (1:50) in a 20 μL PCR system. PCR data were analysis with the comparative CT method ($2^{-\Delta\Delta C_T}$). *Gapdh* or 18s was used

447   as internal controls.

Protein and western blot

449   For extraction of protein from bones, femora were excised free of connecting tissue, flash-

450   frozen and pulverized into bone chips using a pestle and mortar in the presence of liquid

451   nitrogen (while soft tissues were pulverized using a tissue pulverizer (PRIMA, PB100-SP08)),

452   and then digested with protein lysis buffer (Beyotime P0013, supplemented with 1× protease

453   inhibitor cocktail). The lysate was then centrifuged at 12 000 g, 4 °C for 2 minutes and the

454   supernatant was collected. For fractionation of cytoplasmic and nuclear proteins, cell

455   cultures were washed and lysed using the Nuclear and Cytoplasmic Protein Extraction Kit

456   (Beyotime P0028) following the manufacturer's instructions. Protein concentrations were

457   determined using the BCA method.

458   For western blot analysis, protein samples separated by SDS-PAGE were transferred onto

459   PVDF membranes and probed with antibodies against target proteins. Briefly, 20 µg protein

460   samples were electrophoresed at 100V on 5% stacking gel/10% separating gel. After

461   transferred to PVDF membrane (100V, 90 min), and incubated with 5% non-fat milk for

462   30min, the membrane was probed with primary antibodies against MACF1 (1:1000), SMAD7

463   (1:1500), Lamin B1 (1:2000), and GAPDH (1:2000). Washed membranes were then

464   incubated with HRP-conjugated secondary antibodies, and developed and imaged (Gel

465   Doc^{TM} XR+ Gel System).

Immunofluorescence & Cytoskeleton staining

467   Immunofluorescence staining was performed on fibronectin-coated coverslips. Briefly, Cells

468   were plated on coverslips ($1×10^4$/cm^2) and cultured under normal condition for 12h. Then

469   cells were fixed with 4% PFA and rinsed 5 min with TBS, 10 min with TBS-0.5% TritonX-100

470   (TX), and 3×5 min with TBS-0.1%TX, and then blocked with 2% BSA for 10 min. Primary

471   antibodies were added onto each coverslip (10 µL, 1:50), and incubated at 4 °C overnight.

472   The next day, after washed with TBS-0.1%TX, fluorescein-labeled secondary antibodies

473   were added (10 µL, 1:100), and incubated for 1 h. Nucleuses were stained using 5µg/ml

474   DAPI. F-actin were stained using rhodamine phalloidin (ThermoFisher, R415). Mounted

475   coverslips were then examined by confocal microscopy (Leica TCS SP8, Germen).

476   Fluorescent images were analyzed with the FibrilTool (Boudaoud et al., 2014), CytoSpectre

477 (Kartasalo et al., 2015) and Image-Pro Plus.

Co-immunoprecipitation and iTRAQ-LC-MS/MS

479 Co-immunoprecipitation was performed using freshly-harvested MC3T3-E1 cells incubated

480 with antibody recognizing the MACF1 protein. Briefly, cells were harvested in RIPA buffer.

481 Whole cell lysates were incubated at 4°C overnight with 4 μg anti-MACF1 antibody (Abcam,

482 ab117418) or 2 μg Rabbit IgG (Abcam, ab46540). The antigen/antibody complexes were

483 then mixed with 40 μL recombinant Protein A+G agarose beads (Beyotime, P2055), and

484 incubated for 2 h at room temperature. Immunocomplexes were then centrifuged at 1000 g

485 for 5 min to remove supernatant, and then beads complexes were washed with RIPA buffer

486 for 5 times. After washing, beads complexes were resuspended with 20 μL 1X SDS-PAGE

487 electrophoresis loading buffer, and bound proteins were retrieved from agarose beads by

488 boiling for 5 min.

489 For analysis of MACF1-interacting proteins, co-immunoprecipitated products were labeled

490 with iTRAQ reagents and subjected to LC-MS/MS analysis.

Cleared skeleton preparation

492 Fetuses or neonatal mice were euthanized by anesthetization (pentobarbital sodium, i.p.,

493 0.5 g/Kg). Samples were skinned and eviscerated before being fixed in 95% ethanol for 24

494 h, and then incubated in acetone overnight. To stain for cartilage, samples were rinsed with

495 water for 3 changes and left in 0.03% (w/v) Alcian blue solution for about 18 h (depending

496 on the development stage of the samples), and then cleared in 1% KOH until soft tissues

497 were hardly visible. To visualize calcified bone, samples were counterstained in 0.02%

498 Alizarin Red S solution for about 12 h, and then cleared in 1% KOH. Images were acquired

499 by a digital camera, and dimensional parameters were acquired using Image-Pro Plus.

Bone Densitometry & Micro-computed tomography

501 Bone mineral density was measured using a high resolution dual-energy X-ray imaging

502 system (MEDIKORS, InAlyzer, 55KeV and 80Kev). Microarchitecture and stereological

503 parameters were acquired using an micro-computed tomography instrument (EL-SP, GE,

504 80 kPV, 80 μA, 3000 ms) at an isotropic resolution of 8 μm. Data were then reconstructed

505 at a voxel size of 16×16×16 μm. Stereological parameters of the trabeculae were measured

506 within a 1 mm-high region above the distal femur epiphyseal plate using MicroView (a GE

17

507 distribution). Sample scanning and data analysis adhered to a previous protocol (Bouxsein

508 et al., 2010). Additional parameters were acquired using ImageJ and Image-Pro Plus.

509 **Three-point bending test**

510 Mechanical properties of the femur were tested by means of 3-point bending using an

511 universal test machine (Instron 5943). Briefly, freshly-dissected femora were cleaned free of

512 connective tissue and wrapped in normal saline-soaked gauze and kept moist at 4 °C. For

513 subsequent test, femora were secured to the lower supporting pins (span: 9 mm, fillet radius:

514 1 mm) one by one. After preloaded with 1N for 5 s, the tissues were loaded to failure at 1.5

515 mm/min, and load-displacement curves were collected. The inner and outer diameters of

516 the loaded femora were measured using a 3D digital microscope (Hirox KH-8700, Japan).

517 Mechanical parameters were acquired using a built-in software and a previous reported

518 method (Sharir et al., 2008).

519 **Histochemical, calcein labeling and histomorphometric analysis**

520 Formalin-fixed paraffin-embedded (FFPE) tissue sections were prepared and stained using

521 conventional methods. Briefly, fresh tissue were fixed in 4% PFA, decalcified in 10% EDTA

522 (for femoral FFPE sections only), dehydrated through graded ethanol, and embedded into

523 paraffin. Sections were obtained at 4 µm. HE, ALP staining (0.5% β-glycerophosphate

524 Disodium + 0.5% Barbital sodium + 0.5% $CaCl_2$ + 0.5% Mg_2SO_4 + 2% cobalt nitrate + 1%

525 ammonium sulfide) and TRAP staining (50mM $C_4H_{12}KNaO_{10}$) were performed on serial

526 sections. Stained sections were then scanned using a digital slide scanner (Aperio AT2,

527 Leica, German).

528 For plastic embedded sections, 6-week-old mice were injected intraperitoneally with calcein

529 (10 mg/kg) 10 days and 2 days prior to euthanasia, respectively. Femora were then collected

530 and fixed, and embedded in gradient methyl methacrylate after conventional tissue

531 dehydration and clearing. Sections (~20 µm) were prepared using the EXAKT 300CP tissue

532 cutting systems and stained using modified Goldner's trichrome staining method (Gruber,

533 1992). Slides were visualized using a phase contrast microscope (OSTEO-SCAN). For

534 histomorphometric parameters, images were analyzed using Histomorph suite (van 't Hof et

535 al., 2017) and Image-Pro Plus.

18

Serological factors

Whole blood collected by cardiac puncture was used for serum separation. Serological factors were detected by means of enzyme-linked immunosorbent assay following the manufacturer's instructions (Cloud-Clone Corp.). O.D. values were read at 450 nm (BioTek Synergy HT, VT, USA).

Cell culture staining

Von Kossa staining was performed using 5% $AgNO_3$ after being induced for 21 days. ALP staining was performed using a BCIP/NBT alkaline phosphatase color development kit (Beyotime, C3206) following to the manufacturer's instructions. Briefly, cell cultures were washed with cold PBS, fully fixed in 4% PFA and washed. The staining working solution was prepared by mixing BCIP (5-Bromo-4-chloro-3-indolyl phosphate, 300×) and NBT (nitro blue tetrazolium chloride, 150×) into the color developing buffer, cell cultures were then stained in the dark for 15 min. Nodules formation staining was performed using 0.5% Alizarin Red S solution (ARS). Stained cell culture plates were scanned using a digital scanner (CanoScan 9000F MarkII, Japan).

Electric Cell-Substrate Impedance Sensing

Dynamic physiological properties of MSCs during proliferation and differentiation were monitored non-invasively using the ECIS Zθ system (Applied BioPhysics, Troy, NY) (Bagnaninchi and Drummond, 2011). Briefly, cells plated onto fibronectin-coated (20 µg/mL) standard 8-well array (8W10E+) were supplemented with 400 µL growth medium, and cultured in CO_2 incubator for 6 h before initial test. To measure impedance values of differentiating MSCs, growth medium was replaced with osteogenic osteo-induction medium, and data were collected every 80 s at a current frequency of 64 kHz.

Plasmid preparation

The SMAD7 overexpression vector was cloned into the pcDNA3 backbone. Briefly, double enzyme digestion was performed on selected restriction enzyme sites. Then, seamless clone-specific primers were designed to match selected restriction enzyme sites, and the SMAD7 CDS sequence was amplified by PCR. Products from the aboved steps were purified by gel extraction. Linearized vector and CDS insert were recombined in the presence of high-fidelity polymerase. The recombinants were then transformed into Stbl3

19

competent cells and sequenced. Endotoxin-free plasmid was prepared and transfected into cells using nano particle transfection reagent (Engreen H4000) according to the manufacturer's instructions.

Data processing & Statistics

Image acquisition equipments include phase contrast microscope, fluorescence microscope, confocal microscope, digital camera, digital scanner, digital slide scanner, gel imaging system, micro-computed tomography, and dual-energy X-ray absorptiometry. To ease observation and statistical analysis, certain images may have been pre-processed using Adobe® Photoshop®. Operations applied to image data include cropping, scaling, flipping, background clearing, local zoom in and tagging. Other lossy operations such as brightness adjustment, contrast adjustment, levels adjustment were applied only to a limited number of images simultaneously, and great efforts were made to ensure that these operations did not change the essence or any measurable variables of the images.

All data are presented as mean ± s.d. Statistical significance between two groups were determined using Student's t-test. A P-value less than 0.05 was considered statistically significant.

ACKNOWLEDGMENTS

AUTHOR CONTRIBUTIONS

Conceptualization, F.Z., X.M. and A.Q.; Methodology, F.Z., X.M., W.Q., Z.C., P.H., C.Y.; Formal Analysis, F.Z., J.M.; Investigation, F.Z., X.M., W.Q., P.W., R.Z., Z.C., P.H., L.C., C.Y.; Writing -Original Draft, F.Z.; Supervision, A.Q., G.Z.; Project Administration, A.Q., G.Z., Y.L.; Funding Acquisition, A.Q., L.H., Y.T., X.L.

CONFLICTS OF INTEREST

The authors declare no conflicts of interest.

REFERENCES

Antonellis PJ, Pollock LM, Chou S-W, Hassan A, Geng R, Chen X, Fuchs E, Alagramam KN, Auer M, McDermott BM. 2014. ACF7 Is a Hair-Bundle Antecedent, Positioned to Integrate Cuticular Plate Actin and Somatic Tubulin. *J Neurosci* **34**:305–312. doi:10.1523/JNEUROSCI.1880-13.2014

Bagnaninchi PO, Drummond N. 2011. Real-time label-free monitoring of adipose-derived stem cell differentiation with electric cell-substrate impedance sensing. *Proc Natl Acad Sci U S A* **108**:6462–7. doi:10.1073/pnas.1018260108

Bernier G, Mathieu M, De Repentigny Y, Vidal SM, Kothary R. 1996. Cloning and characterization of mouse ACF7, a novel member of the dystonin subfamily of actin binding proteins. *Genomics* **38**:19–29.

Boudaoud A, Burian A, Borowska-Wykręt D, Uyttewaal M, Wrzalik R, Kwiatkowska D, Hamant O. 2014. FibrilTool, an ImageJ plug-in to quantify fibrillar structures in raw microscopy images. *Nat Protoc* **9**:457–63. doi:10.1038/nprot.2014.024

Bouxsein ML, Boyd SK, Christiansen BA, Guldberg RE, Jepsen KJ, Müller R. 2010. Guidelines for assessment of bone microstructure in rodents using micro-computed tomography. *J Bone Miner Res* **25**:1468–86. doi:10.1002/jbmr.141

Chen H-J, Lin C-M, Lin C-S, Perez-Olle R, Leung CL, Liem RKH. 2006. The role of microtubule actin cross-linking factor 1 (MACF1) in the Wnt signaling pathway. *Genes Dev* **20**:1933–45. doi:10.1101/gad.1411206

Duhamel S, Goyette M-A, Thibault M-P, Filion D, Gaboury L, Côté J-F. 2018. The E3 Ubiquitin Ligase HectD1 Suppresses EMT and Metastasis by Targeting the +TIP ACF7 for Degradation. *Cell Rep* **22**:1016–1030. doi:10.1016/j.celrep.2017.12.096

Elefteriou F, Yang X. 2011. Genetic mouse models for bone studies—Strengths and limitations. *Bone* **49**:1242–1254. doi:10.1016/j.bone.2011.08.021

Emori T, Kitamura K, Okazaki K. 2012. Nuclear Smad7 Overexpressed in Mesenchymal Cells Acts as a Transcriptional Corepressor by Interacting with HDAC-1 and E2F to Regulate Cell Cycle. *Biol Open* **1**:247–60. doi:10.1242/bio.2012463

Escobar-Aguirre M, Zhang H, Jamieson-Lucy A, Mullins MC. 2017. Microtubule-actin crosslinking factor 1 (Macf1) domain function in Balbiani body dissociation and nuclear positioning. *PLOS Genet* **13**:e1006983. doi:10.1371/journal.pgen.1006983

Fassett JT, Xu X, Kwak D, Wang H, Liu X, Hu X, Bache RJ, Chen Y. 2013. Microtubule Actin Cross-linking Factor 1 regulates cardiomyocyte microtubule distribution and adaptation to hemodynamic overload. *PLoS One* **8**:e73887. doi:10.1371/journal.pone.0073887

Goryunov D, He C-Z, Lin C-S, Leung CL, Liem RKH. 2010. Nervous-tissue-specific elimination of microtubule-actin crosslinking factor 1a results in multiple developmental defects in the mouse brain. *Mol Cell Neurosci* **44**:1–14. doi:10.1016/j.mcn.2010.01.010

Gruber HE. 1992. Adaptations of Goldner's Masson trichrome stain for the study of undecalcified plastic embedded bone. *Biotech Histochem* **67**:30–4.

Hilton MJ. 2014. Skeletal development and repair: methods and protocols.

Hornbeck P V., Zhang B, Murray B, Kornhauser JM, Latham V, Skrzypek E. 2015. PhosphoSitePlus, 2014: mutations, PTMs and recalibrations. *Nucleic Acids Res* **43**:D512–D520. doi:10.1093/nar/gku1267

Hu L, Su P, Li R, Yan K, Chen Z, Shang P, Qian A. 2015. Knockdown of microtubule actin crosslinking factor 1 inhibits cell proliferation in MC3T3-E1 osteoblastic cells. *BMB Rep* **48**:583–8.

Hu L, Su P, Yin C, Zhang Y, Li R, Yan K, Chen Z, Li D, Zhang G, Wang L, Miao Z, Qian A, Xian CJ. 2017.

640   Microtubule actin crosslinking factor 1 promotes osteoblast differentiation by promoting β-
641   catenin/TCF1/Runx2 signaling axis. *J Cell Physiol*. doi:10.1002/jcp.26059

642 Ka M, Jung E-M, Mueller U, Kim W-Y. 2014. MACF1 regulates the migration of pyramidal neurons via
643   microtubule dynamics and GSK-3 signaling. *Dev Biol* **395**:4–18. doi:10.1016/j.ydbio.2014.09.009

644 Ka M, Kim W-Y. 2016. Microtubule-Actin Crosslinking Factor 1 Is Required for Dendritic Arborization and
645   Axon Outgrowth in the Developing Brain. *Mol Neurobiol* **53**:6018–6032. doi:10.1007/s12035-015-9508-
646   4

647 Ka M, Moffat JJ, Kim W-Y. 2016. MACF1 Controls Migration and Positioning of Cortical GABAergic
648   Interneurons in Mice. *Cereb Cortex*. doi:10.1093/cercor/bhw319

649 Kakinuma T, Ichikawa H, Tsukada Y, Nakamura T, Toh B-H. 2004. Interaction between p230 and MACF1 is
650   associated with transport of a glycosyl phosphatidyl inositol-anchored protein from the Golgi to the cell
651   periphery. *Exp Cell Res* **298**:388–398. doi:10.1016/j.yexcr.2004.04.047

652 Kartasalo K, Pölönen R-P, Ojala M, Rasku J, Lekkala J, Aalto-Setälä K, Kallio P. 2015. CytoSpectre: a tool
653   for spectral analysis of oriented structures on cellular and subcellular levels. *BMC Bioinformatics*
654   **16**:344. doi:10.1186/s12859-015-0782-y

655 Khurana JS. 2009. Bone pathology. Humana Press.

656 Kodama A, Karakesisoglou I, Wong E, Vaezi A, Fuchs E. 2003. ACF7: an essential integrator of microtubule
657   dynamics. *Cell* **115**:343–54.

658 Lane TR, Fuchs E, Slep KC. 2017. Structure of the ACF7 EF-Hand-GAR Module and Delineation of
659   Microtubule Binding Determinants. *Structure* **25**:1130-1138.e6. doi:10.1016/j.str.2017.05.006

660 Leung CL, Sun D, Zheng M, Knowles DR, Liem RK. 1999. Microtubule actin cross-linking factor (MACF): a
661   hybrid of dystonin and dystrophin that can interact with the actin and microtubule cytoskeletons. *J Cell*
662   *Biol* **147**:1275–86.

663 Li N, Lee WY-W, Lin S-E, Ni M, Zhang T, Huang X-R, Lan H-Y, Li G. 2014. Partial loss of Smad7 function
664   impairs bone remodeling, osteogenesis and enhances osteoclastogenesis in mice. *Bone* **67**:46–55.
665   doi:10.1016/j.bone.2014.06.033

666 Liang Y, Shi C, Yang J, Chen H, Xia Y, Zhang P, Wang F, Han H, Qin H. 2013. ACF7 regulates colonic
667   permeability. *Int J Mol Med* **31**:861–6. doi:10.3892/ijmm.2013.1284

668 Logan M, Martin JF, Nagy A, Lobe C, Olson EN, Tabin CJ. 2002. Expression of Cre Recombinase in the
669   developing mouse limb bud driven by a Prxl enhancer. *Genesis* **33**:77–80. doi:10.1002/gene.10092

670 Ma Y, Yue J, Zhang Y, Shi C, Odenwald M, Liang WG, Wei Q, Goel A, Gou X, Zhang J, Chen S-Y, Tang W-
671   J, Turner JR, Yang F, Liang H, Qin H, Wu X. 2017. ACF7 regulates inflammatory colitis and intestinal
672   wound response by orchestrating tight junction dynamics. *Nat Commun* **8**:15375.
673   doi:10.1038/ncomms15375

674 May-Simera HL, Gumerson JD, Gao C, Campos M, Cologna SM, Beyer T, Boldt K, Kaya KD, Patel N,
675   Kretschmer F, Kelley MW, Petralia RS, Davey MG, Li T. 2016. Loss of MACF1 Abolishes Ciliogenesis
676   and Disrupts Apicobasal Polarity Establishment in the Retina. *Cell Rep* **17**:1399–1413.
677   doi:10.1016/j.celrep.2016.09.089

678 Miyake T, Alli NS, McDermott JC. 2010. Nuclear function of Smad7 promotes myogenesis. *Mol Cell Biol*
679   **30**:722–35. doi:10.1128/MCB.01005-09

680 Miyazawa K, Miyazono K. 2017. Regulation of TGF-β Family Signaling by Inhibitory Smads. *Cold Spring*
681   *Harb Perspect Biol* **9**:a022095. doi:10.1101/cshperspect.a022095

682 Ning W, Yu Y, Xu H, Liu X, Wang D, Wang J, Wang Y, Meng W. 2016. The CAMSAP3-ACF7 Complex
683   Couples Noncentrosomal Microtubules with Actin Filaments to Coordinate Their Dynamics. *Dev Cell*
684   **39**:61–74. doi:10.1016/j.devcel.2016.09.003

685 Sharir A, Barak MM, Shahar R. 2008. Whole bone mechanics and mechanical testing. *Vet J* **177**:8–17.

686   doi:10.1016/j.tvjl.2007.09.012

687 Slep KC, Rogers SL, Elliott SL, Ohkura H, Kolodziej PA, Vale RD. 2005. Structural determinants for EB1-
688   mediated recruitment of APC and spectraplakins to the microtubule plus end. *J Cell Biol* **168**:587–598.
689   doi:10.1083/jcb.200410114

690 Stehbens S, Wittmann T. 2012. Targeting and transport: How microtubules control focal adhesion dynamics.
691   *J Cell Biol* **198**:481–489. doi:10.1083/jcb.201206050

692 Suozzi KC, Wu X, Fuchs E. 2012. Spectraplakins: master orchestrators of cytoskeletal dynamics. *J Cell Biol*
693   **197**:465–75. doi:10.1083/jcb.201112034

694 van 't Hof RJ, Rose L, Bassonga E, Daroszewska A. 2017. Open source software for semi-automated
695   histomorphometry of bone resorption and formation parameters. *Bone* **99**:69–79.
696   doi:10.1016/j.bone.2017.03.051

697 Wang X, Li N, Xiong N, You Q, Li J, Yu J, Qing H, Wang T, Cordell HJ, Isacson O, Vance JM, Martin ER,
698   Zhao Y, Cohen BM, Buttner EA, Lin Z. 2017. Genetic Variants of Microtubule Actin Cross-linking Factor
699   1 (MACF1) Confer Risk for Parkinson's Disease. *Mol Neurobiol* **54**:2878–2888. doi:10.1007/s12035-
700   016-9861-y

701 Wu M, Chen G, Li Y-P. 2016. TGF-β and BMP signaling in osteoblast, skeletal development, and bone
702   formation, homeostasis and disease. *Bone Res* **4**:16009. doi:10.1038/boneres.2016.9

703 Wu X, Kodama A, Fuchs E. 2008. ACF7 regulates cytoskeletal-focal adhesion dynamics and migration and
704   has ATPase activity. *Cell* **135**:137–48. doi:10.1016/j.cell.2008.07.045

705 Yin C, Zhang Y, Hu L, Tian Y, Chen Z, Li D, Zhao F, Su P, Ma X, Zhang G, Miao Z, Wang L, Qian A, Xian
706   CJ. 2018. Mechanical unloading reduces microtubule actin crosslinking factor 1 expression to inhibit β-
707   catenin signaling and osteoblast proliferation. *J Cell Physiol* **233**:5405–5419. doi:10.1002/jcp.26374

708 Yue J, Zhang Y, Liang WG, Gou X, Lee P, Liu H, Lyu W, Tang W-J, Chen S-Y, Yang F, Liang H, Wu X.
709   2016. In vivo epidermal migration requires focal adhesion targeting of ACF7. *Nat Commun* **7**:11692.
710   doi:10.1038/ncomms11692

711 Zhang Y, Yin C, Hu L, Chen Z, Zhao F, Li D, Ma J, Ma X, Su P, Qiu W, Yang C, Wang P, Li S, Zhang G,
712   Wang L, Qian A, Xian CJ. 2018. MACF1 Overexpression by Transfecting the 21 kbp Large Plasmid
713   PEGFP-C1A-ACF7 Promotes Osteoblast Differentiation and Bone Formation. *Hum Gene Ther* **29**:259–
714   270. doi:10.1089/hum.2017.153

715 Zhu H, Guo Z-K, Jiang X-X, Li H, Wang X-Y, Yao H-Y, Zhang Y, Mao N. 2010. A protocol for isolation and
716   culture of mesenchymal stem cells from mouse compact bone. *Nat Protoc* **5**:550–60.
717   doi:10.1038/nprot.2009.238

718

719   **FIGURE LEGENDS**

Figure 1

720
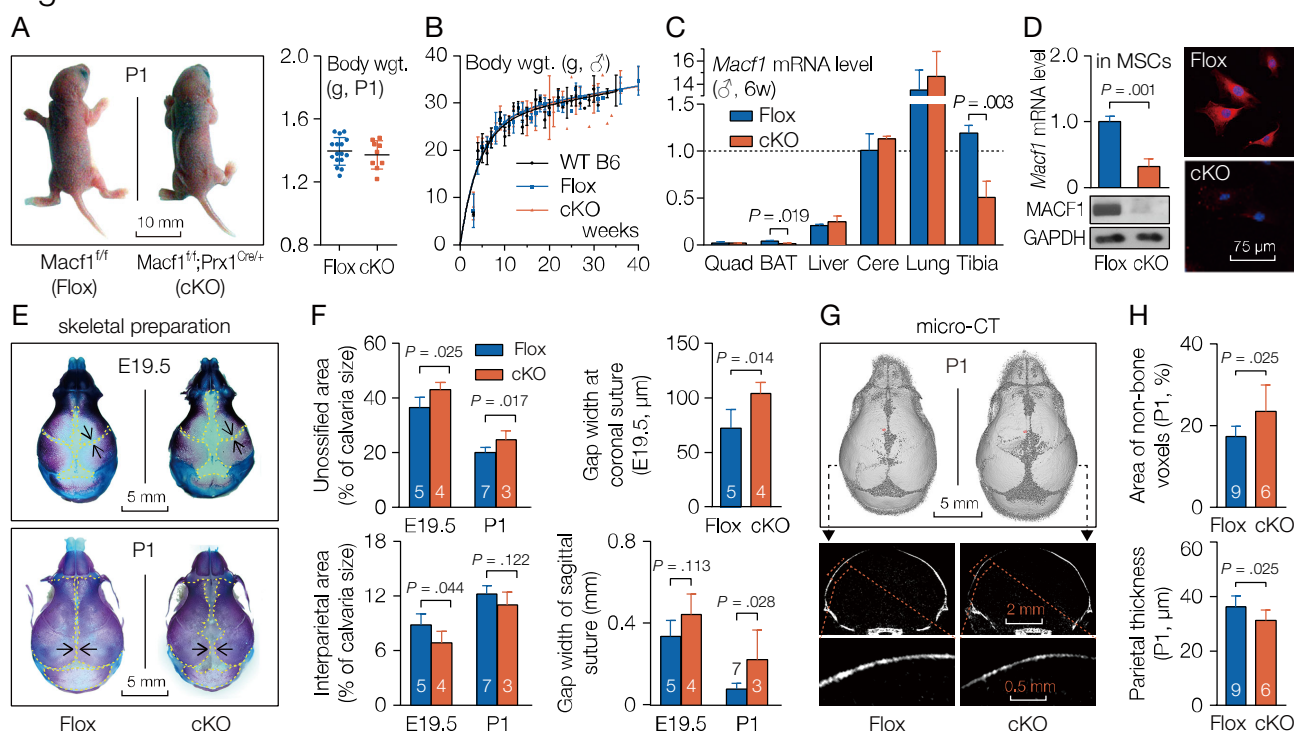
Fig. 1. Mesenchymal deletion of MACF1 retards early stage bone development in mice. (A) Representative images and body weight of neonatal MACF1 cKO mice (P1, postnatal day 1). (B) Growth curve of male MACF1 cKO mice. Least-squares fitting Gompertz function was used. (C) Real-time quantitative PCR analysis of *Macf1* mRNA levels in organs or tissues of MACF1 cKO mice (6-week old, male). Quad, quadriceps. BAT, brown adipose tissue. Cere, cerebrum. (D) Expression and distribution of MACF1 in MACF1 deficient MSCs. *Gapdh*/GAPDH were used as internal reference. (E) Representative images of cleared skeletal preparation showing early-stage development of the skull (E19.5, embryonic day 19.5). Red shows ossified tissue, while blue indicates cartilage (dashed lines). (F) Quantification of panel E. Gap width indicates the nearest distance between adjacent bones. (G) Representative 3D reconstruction images showing skull development at P1. Cross-sections of the parietal bone are also shown. (H) Quantification of panel G; Non-bone voxels indicate unossified part. Data are represented as mean ± s.d. Significances were determined using student's *t*-test.
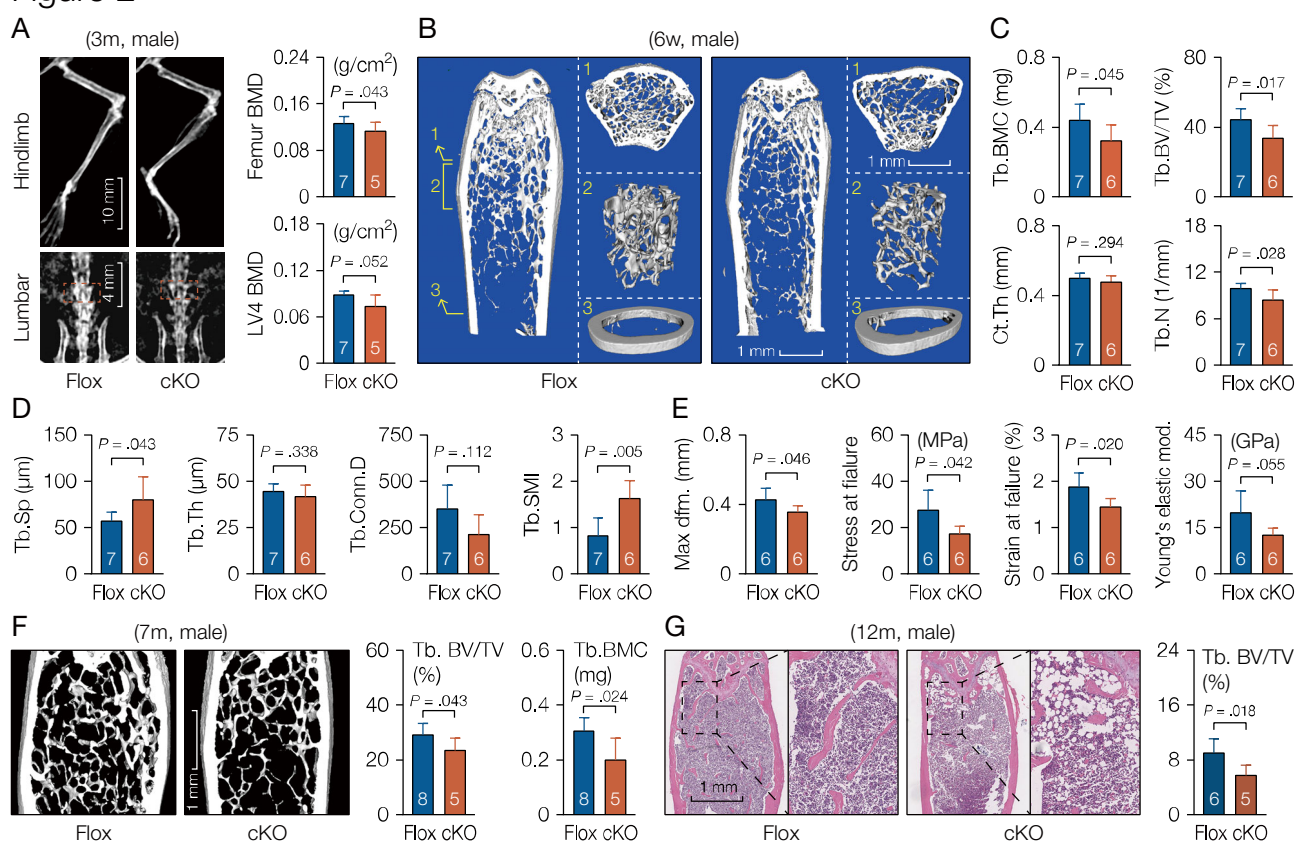
24

Figure 2

Fig. 2. Mesenchymal deletion of MACF1 weakens bone properties in adult mice. (A) X-ray images of MACF1 cKO mice (male, 3-month old). BMD of femur and third lumbar vertebra were quantified. (B) Representative 3D reconstruction images showing microarchitecture of distal femur (male, 6-week old). Positions of reconstructed region are indicated by Arabic numerals. (C and D) Stereological parameters for trabecular and cortical bone in distal femur. BMC, bone mineral content; BV/TV, bone volume fraction; Ct.Th, cortical thickness; Ct.Ar, cortical area. Tb.N, trabecular number; Tb.Sp, trabecular spacing; Tb.Th, trabecular thickness; SMI, structural model index. Conn.D, connectivity density. (E) Femoral mechanical property (male, 3-month old). Max dfm., maximum deformation; Young's mod., Young's elastic modulus. (F) MicroCT analysis of distal femur (male, 7-month old). (G) Representative images of H&E staining showing trabecular in distal femur (12-month old, male, coronal sections). Bone volume fraction was quantified. Data are represented as mean ± s.d. Statistical significance were determined using student's t-test.
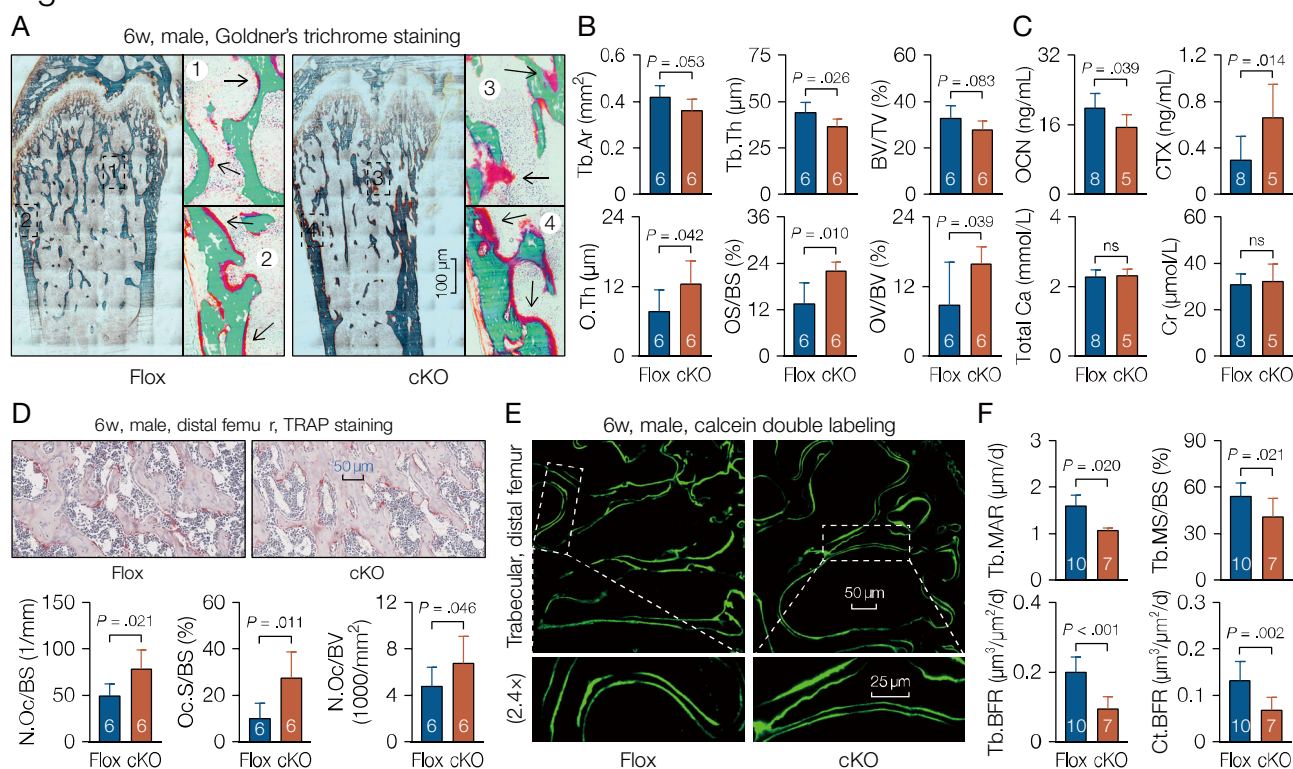
25

Figure 3

Fig. 3. Low bone formation capacity in MACF1 cKO mice. (A) Representative images of Goldner's trichrome staining showing mineralized matrix and osteoid in femur (male, 6-week old, coronal sections). Green shows mineralized bone, while red indicates osteoid. Numbered boxes are enlarged to show details. (B) Quantification of panel A. OV/BV, osteoid volume to trabecular bone volume. OS/BS, osteoid surface to trabecular bone surface. O.Th, average osteoid thickness. (C) Sandwich enzyme immunoassay for *in vitro* quantification of serological factors. OCN, osteocalcin; CTX, carboxy-terminal collagen crosslinks; Cr, creatinine. (D) Representative images of TRAP staining showing bone resorption in femur (male, 6-week old, coronal sections). N.Oc/BS, number of osteoclasts per bone surface; Oc.S/BS, osteoclast surface per bone surface; N.Oc/BV, number of osteoclasts per bone volume. (E) Representative images of calcein double labeling showing mineral apposition and bone formation in femur (male, 6-week old, coronal sections). Boxed regions are enlarged. (F) Quantification of panel E. MAR, mineral apposition rate; MS/BS, mineralizing surface per bone surface; BFR, bone formation rate per bone surface. Data are represented as mean ± s.d. Statistical significance were determined using student's *t*-test.
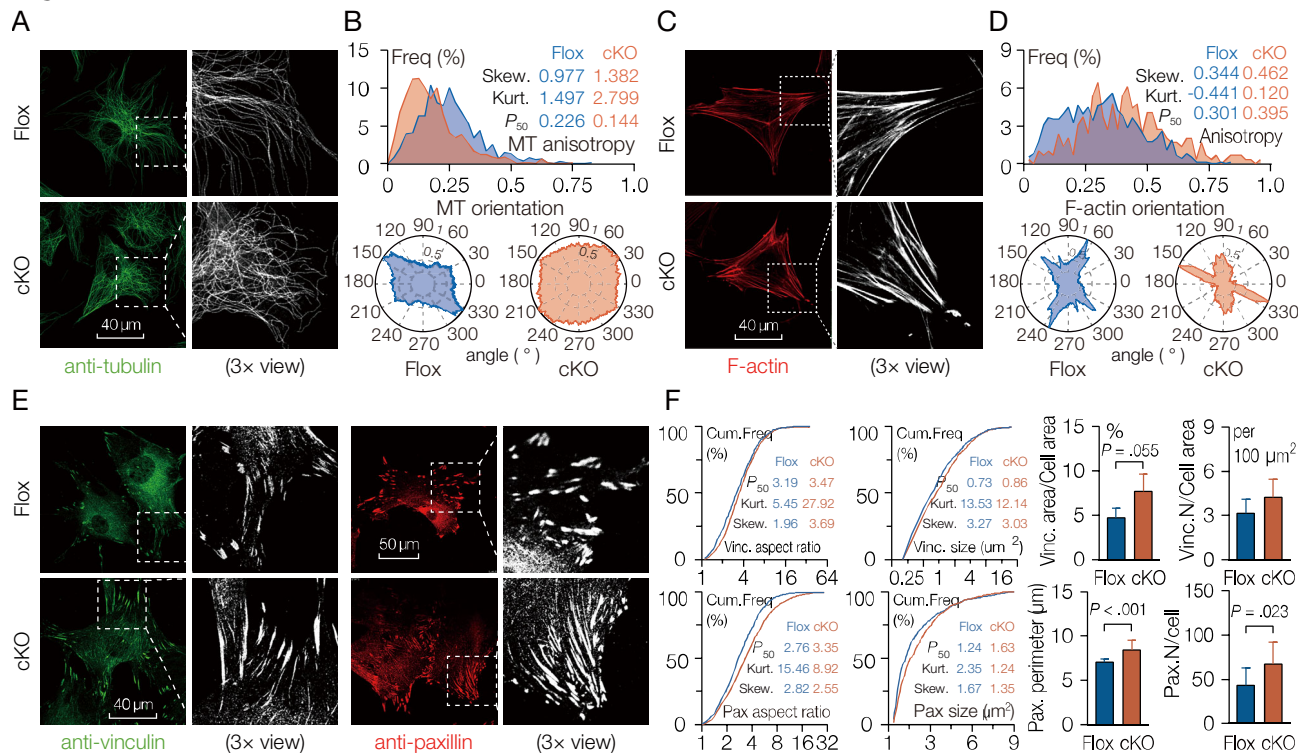
Figure 4

Fig. 4. Loss of MACF1 alters the organization of cytoskeleton in MSCs. (A) Representative immunostaining images of MACF1 deficient MSCs stained with antibody recognizing alpha-tubulin. (B) Anisotropy and orientation of the microtubule cytoskeleton. MT, microtubule; Skew., skewness; Kurt., kurtosis; P_{50}, median. (C) Representative immunostaining images of MSCs stained with rhodamine-conjugated phalloidin. (D) Anisotropy and orientation of the actin cytoskeleton. (E) Representative immunostaining images of MSCs stained with antibodies recognizing vinculin or paxillin to show focal adhesions. (F) Size and morphometric parameters of vinculin (Vinc.) or paxillin (Pax.) plaque. Cum.Freq, cumulative frequency. Data are represented as mean ± s.d. Statistical significance were determined using student's t-test.

Figure 5
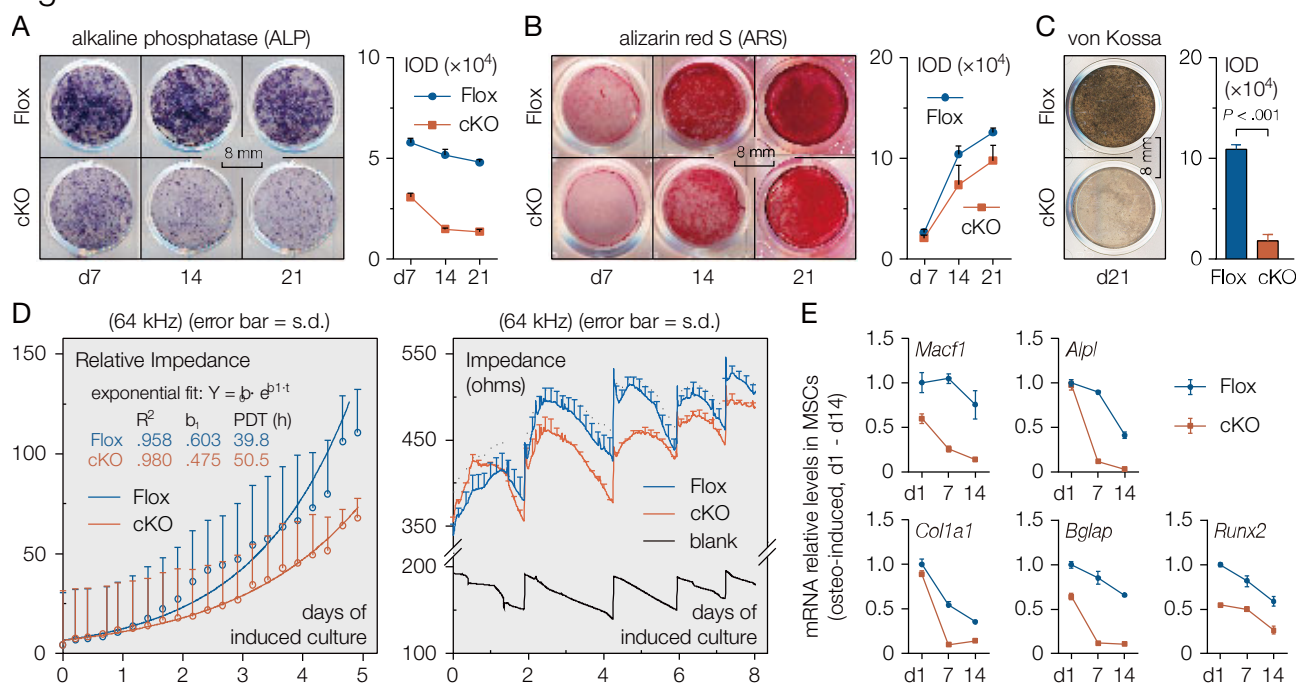
Fig. 5. Loss of MACF1 inhibits osteoblastic differentiation in MSCs. (A) Representative images of von Kossa staining showing mineralization capacity after osteo-induced for 21 days. Staining intensity was quantified as IOD (integrated optical density). (B and C) Representative staining images showing alkaline phosphatase expression and mineralized nodules formation in MSCS during osteo-induced culture. (D) Real-time impedance curve showing proliferation and differentiation capability of MSCs during osteo-induced culture. PDT, population doubling time. (E) Real-time PCR analysis of osteogenic marker gene expression during osteo-induced culture. Data are represented as mean ± s.d.
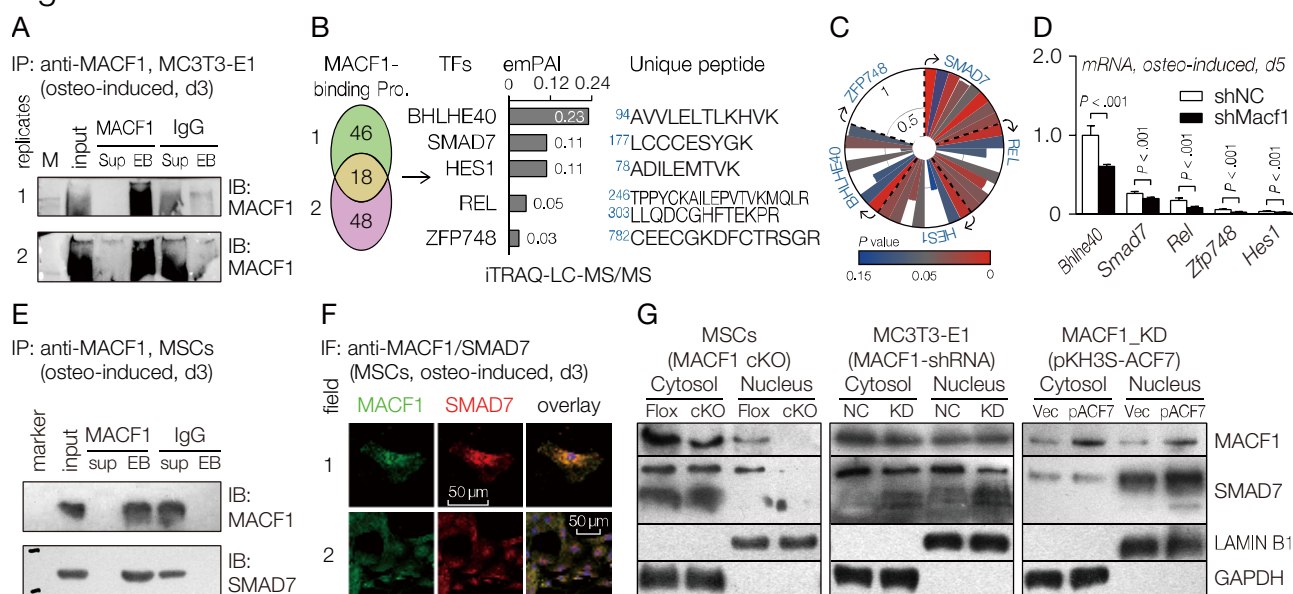
Figure 6

Fig. 6. MACF1 interacts with SMAD7. (A) Co-immunoprecipitated products using anti-MACF1 antibody for iTRAQ analysis. (B) MACF1-interacting proteins identified by co-immunoprecipitation coupled LC-MS/MS assay, abundance of MACF1-interacting transcriptional factors (TFs) and unique peptide sequence (positions marked by Arabic numerals) were also provided. emPAI, exponentially modified protein abundance index. (C) Potential of candidate TFs to be involved in osteogenic differentiation. Radial coordinates represent the *Score* values predicted by ToppGene database, while angular coordinates show 8 predicted items (clockwise: GO: Molecular Function; GO: Biological Process; GO: Cellular Component; Human Phenotype; Mouse Phenotype; Pathway; Pubmed; Disease). (D) Real-time PCR analysis of candidate TFs in MACF1 knockdown MC3T3-E1 preosteoblasts after osteo-induced for 5 days. (E) Co-immunoprecipitation assay to detect the association of MACF1 with SMAD7. MSCs were co-immunoprecipitated using anti-MACF1 antibody or IgG. (F) Expression and distribution of MACF1 and SMAD7 in normal MSCs after induced. (G) Western blot analysis of MACF1 and SMAD7 levels in MACF1 cKO MSCs, MACF1 knockdown preosteoblasts, and MACF1 stable transfected MACF1 knockdown preosteoblasts. ACF7 (Actin cross-linking family protein 7) is a synonym for MACF1. Lamin B1 and GAPDH were used as internal reference for nucleus and cytoplasm, respectively. Data are represented as mean ± s.d. Statistical significance were determined using student's *t*-test.
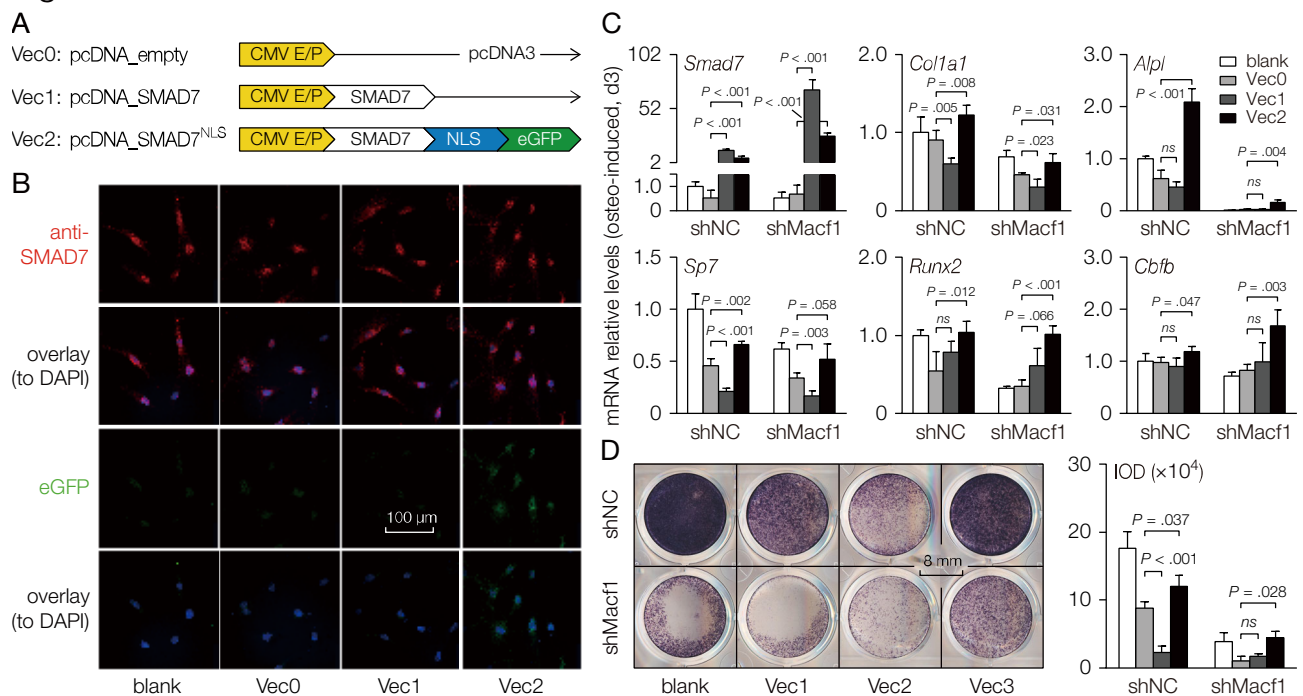
29

Figure 7

Fig. 7. MACF1 facilitate SMAD7 nucleus translocation to drive osteoblastic differentiation. (A). Schematic diagram of the SMAD7 expression plasmids. The mouse SMAD7 coding sequence was cloned into pdDNA3 backbone. NLS, nuclear localization sequence (SV40 large T antigen). (B) Representative immunostaining images of MC3T3-E1 preosteoblasts showing SMAD7 (red) and eGFP (green) expression after plasmid transfection. Blank group was not transfected. (C) Real-time PCR analysis of relative gene expression of Smad7, osteogenic marker genes and osteogenic-related TFs in *Macf1* knockdown MC3T3-E1 preosteoblasts after plasmid transfection. (D) Representative staining images showing alkaline phosphatase expression in *Macf1* knockdown MC3T3-E1 preosteoblasts after plasmid transfection. Data are represented as mean ± s.d. Statistical significance were determined using student's *t*-test.

30

Working model

817
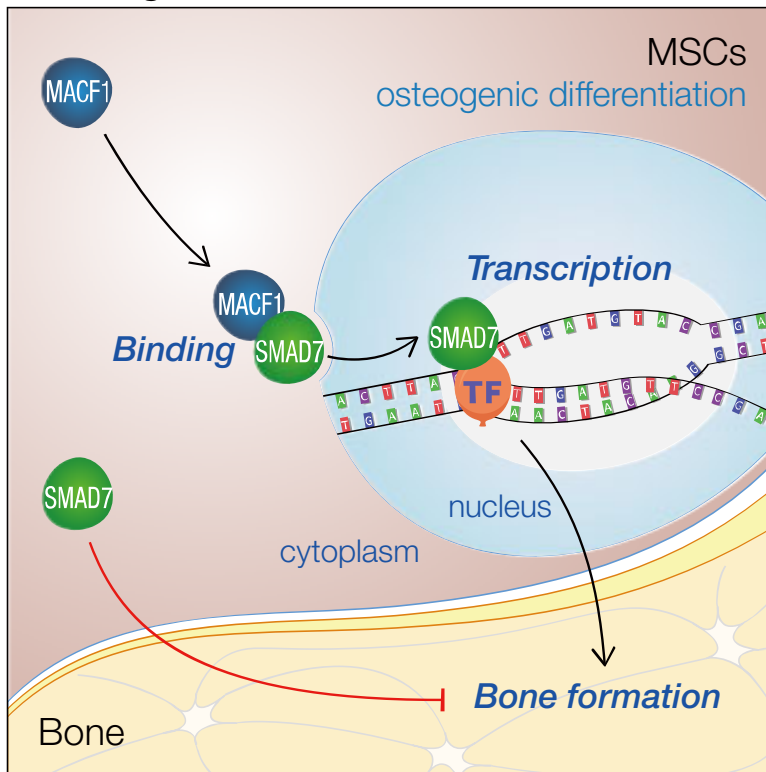
Working model. MACF1 is essential for maintaining osteogenic differentiation and bone formation. In MSCs, cytoplasmic SMAD7 inhibits osteogenic differentiation, while MACF1 promotes nuclear translocation of SMAD7 to initiate osteogenic pathways.